Computational Sciences and Engineering 5(1) (2025) 71-95

University of Guilan

Computational Sciences and Engineering

journal homepage: https://cse.guilan.ac.ir/

Computational Fluid Dynamics (CFD) Modelling of Ventilation Air Mixed with Aerosol Sanitizer Flow: Case Study of a Health Care Facility

Vahid Gholami Motlagh [a], Mohammad Ahmadzadehtalatapeh [a,*]

[a] Department of Mechanical Engineering, Chabahar University of Maritime and Marine Sciences, Chabahar, Iran

ARTICLE INFO

Article history:
Received 4 May 2025
Received in revised form 9 July 2025
Accepted 2 September 2025
Available online 2 September 2025

Keywords:
CFD analysis
Indoor Virus
Surgery Room
Ventilation System

ABSTRACT

Indoor viruses are transmitted by inhalation with droplet nuclei produced by an infected person during coughing, sneezing, and speaking. In addition, the risk of airborne droplet nuclei in indoor environments, especially in health care facilities is significant. In this study, the feasibility of eliminating the indoor viruses with mixing the ventilation system air with an aerosol sanitizer flow in a surgical room (SR) was investigated using CFD analysis. Indoor thermal comfort and energy utilization coefficient (EUC) were also investigated. Four cases with different inlet configurations and related air distribution patterns were analyzed. The simulation results showed that the SR with an inlet system in the side wall has a significant ability to mix aerosol sanitizer flow with the inlet air (Case 4). It was shown that in Case 4 design, the aerosol sanitizer could reach any point in the room and has the potential to eliminate the indoor viruses, thus would protect the patient and surgical staff from the risk of infection. It was also revealed that Case 4 is capable of establishing acceptable indoor thermal comfort conditions and also highest EUC value belongs to Case 4.

1. Introduction

One of the most common ways in the indoor environment for people to be infected by viruses is through exposure to the viruses [1, 2]. In addition, airways are one of the primary routes of transmission for droplets and aerosol dispersion in the indoor environment [3]. Moreover, controlling the indoor space is essential for reducing the risk of contamination in indoor environments. Heating, ventilation, and air-conditioning (HVAC) systems are used to provide thermal comfort and ensure a safe indoor environment [1, 4]. Therefore, the rational use of HVAC systems for environmental control is of high importance to reduce the risk of infection and

* Corresponding author.
E-mail addresses: m_ahmadzadeh56@yahoo.com (M. Ahmadzadehtalatapeh)

https://doi.org/10.22124/cse.2025.30579.1104

improve human wellbeing [1]. HVAC systems help to maintain thermal comfort and indoor air quality by removing indoor air contaminants and providing fresh air for the occupants [1, 5]. Indoor air quality and thermal comfort in the hospital environment affect the patient and staff health [6-8]. Moreover, inappropriate thermal conditions in a surgical room (SR) environment are essential and may reduce work efficiency and increase the possibility of surgical errors [9]. Extensive research studies have been conducted on the use of air conditioning systems to eliminate and minimize the virus transmission [10-14]. For instance, Sadrizadeh et al. [12] analyzed the effect of the surgeon's posture on the distribution of airborne particle in an operating theater with turbulent mixing ventilation. Two different positions, namely bending and straightening were examined, which indicated the common positions of the surgeon and surgical staff. Ultraclean-zoned ventilation systems were examined. In this study, the mentioned system was used as an addition to the conventional operating theater. The results showed that ultraclean-zoned ventilation systems are effective in reducing the deposition and concentration of bacteria-carrying particle. It was also found that the poor situation of surgical staff can significantly reduce the efficiency of these systems. Romano et al. [13] performed numerical and experimental analysis on the airborne particles control in a SR. In this study, the effectiveness of a differential air flow diffusion system on reducing the concentration of particles above the operating table was explored. It was shown that the differential air flow diffusion system is able to maintain the desired protective effect against contamination load. Gholami Motlagh et al. [14, 15] studied air distribution in a SR with different inlet and outlet patterns. In this study, the environmental parameters and contamination released from the patient and surgical staff were analyzed. The study showed that creating unidirectional flow by laminar airflow systems is very successful in reducing contamination of the surgical zone. Liu et al. [16] investigated the effects of a circulating health care staff (nurse) moving in the operating room on airflow pattern and particles with bacteria. The results showed that while the health care staff was not moving, thermal plume of surgical staff and surgical lamps have a significant effect on air distribution. Therefore, the concentration of bacteria-carrying particles (BCPs) increases. On the other hand, the nurse walked did not change the current state of the airflow. With the increase of nurse's moving speed, the airflow disturbance increases significantly. In addition, the wake length behind the staff increases. It was shown that the circulating nurse did not make any difference in the airflow pattern up the operating table, but due to the circulating nurse passes, BCP concentration level up the nearby instrument tables rises. As a result, the risk of surgical site infections (SSIs) for surgical staff increases. Zhang et al. [17] investigated the effect of air change rate on air quality in a surgical microenvironment in an operating room with mixing ventilation. The study showed that in operating rooms with mixing ventilation, air change rate may determine microbe-carrying particles transmission and indoor air. Experimental measurements of microbe-carrying particles were conducted with different air change rates of 15, 20, and 26. The results showed that the air change rate is the main factor affecting the concentration of microbe-carrying particles. It was also found that the higher exposure risks of surgical incision in the surgical microenvironment may be mitigated with increasing air change rates. Also, significant differences in the concentration of contaminants at exhaust air indicate that the location of medical equipment may affect the efficiency of exhaust. Ho et al. [18] studied the effects of supply and exhaust locations in an operating room, which includes four medical staffs and a patient with a lamp above. The air supply at top of the room over the side walls and the outlets are located at the bottom of the opposite walls. The effect of horizontal air supply and outlet locations on the flow pattern in the operating room was investigated. It was concluded that by placing the air supply close to the center line of the room, better thermal comfort conditions and ventilation performance can be achieved, while the location of the outlets does not make a significant difference. Experimental evaluation of different mixing air ventilation systems on ventilation performance and exposure to exhaled contaminants in hospital rooms were explored by Berlanga et al. [19]. In this study, four different configurations of mixing ventilation in hospital rooms were evaluated in terms of ventilation performance and health workers exposure to contaminants. Three air change rates were examined to determine their effect on the studied variables as: 6, 9 and 12. It was shown that the configuration that the grilles is located in the upper part of a wall leads to high health workers transient exposure values, while the swirl ceiling diffusers configuration maintains low values with increasing air change rates.

In addition, extensive researches have been conducted on the use of HVAC systems to keep people safe from viruses in the indoor spaces. Bhattacharyya et al. [20] performed a computational fluid dynamics (CFD) analysis to minimize viruses in an isolation room. By analyzing the airflow pattern, the effect of mixing an aerosol sanitizer with the inlet air to prevent the medical staff and patients from viruses were investigated. The results showed that creating a flow pattern with a high turbulence field in the isolation room space is an effective way to distribute the sanitizer in the room space and eliminate the viruses. In another study, Ren et al. [21] examined three ventilation strategies with different inlet and outlet designs in a prefabricated inpatient ward. It was illustrated that particles smaller than 20 micrometers could travel with the main flows. On the other hand, the particles larger than 45 micrometers cannot travel with flows and most of them are deposited on surfaces in different areas in any ventilation strategy. It was found that in order to promote the removal of large particles (e.g., 45 μm) by the outlets; the outlets should be installed inside the landing area of large particles and close to the polluted sources. Borro et al. [3] investigated the role of HVAC systems in the diffusion of contagion through CFD simulation of cough at the "Bambino Gesù" Vatican State Children's Hospital. The simulation results for the waiting room showed that the HVAC airflow significantly increases infected droplets diffusion in the indoor space within 25 seconds of cough event. At the same time, it was also observed that due to the HVAC removal, the number of infected droplets decreases. In another study, shao et al. [22] evaluated the risk assessment of airborne transmission of viruses (COVID-19 virus in the research) by asymptomatic individuals. In this study, the output particles from respiratory in spaces such as elevators, small classrooms, and supermarkets were simulated using CFD method. The study was performed to analyze the risk of individuals inhaling virus-infected particles in the mentioned spaces. It was found that modifying the settings of HVAC systems and increasing ventilated spaces significantly increases the potential of removing the contaminated particles. According to the results, the correct choice of individuals' location in the studies cases prevents the concentration of pollution in certain parts of the space. The effect of wind velocity on coughing droplets was investigated by Dbouk et al. [23]. It was proved that when the wind velocity is almost zero, the saliva droplets only travel about 2 meters. The results also showed that at the wind velocity of 4 to 15 km/h, saliva droplets travel more than 6 m in the direction of the wind with reducing the concentration and liquid droplet size. Their findings revealed that the 2 m social distance might not be adequate due to environmental factors. Li et al. [24] evaluated the possibility of airborne virus transmission in a restaurant involving three families. The results showed that viruses can be transmitted through the air in a crowded space with a ventilation rate of 1 L/s per person. On the other hand, preventing overcrowding and proper ventilation and effective air distribution in buildings and transport cabins are very important to prevent the spread of viruses. Vuorinen et al. [25] studied the aerosol transport and the transmission possibility of virus through inhalation of virus-infected air by numerical simulations. The results showed that droplets with a diameter of 50 to 100 microns can remain in the air for about 3 minutes and 20 seconds and could be inhaled by the occupants. The CFD simulations also proved that due to the complexity of airflows, the aerosol is not necessarily evenly distributed in the space. Therefore, such non-uniform expansion certainly affects total exposure. It was found that airflow turbulence causes more people to be exposed to these particles, which increase the risk of occupants' infection.

Many studies have focused on the dispersion of aerosols in indoor environments, particularly during the COVID-19 pandemic. For example, research has shown how ventilation systems can affect the spread of respiratory droplets [1, 20, 21]. Studies show that the effectiveness of aerosol disinfectants depends significantly on factors such as droplet size, airflow velocity, and environmental conditions (humidity and temperature). Research has shown that strategic placement of ventilation systems can increase the distribution of aerosol disinfectants, thereby improving disinfection efficiency [3, 20]. While there is considerable research on aerosol dispersion, fewer studies have examined CFD simulations to evaluate the dynamic behavior of aerosol disinfectants in air mixing [1, 3, 20, 26]. There is also a need for more comprehensive studies that consider various environmental factors and their impact on the effectiveness of aerosol disinfectants. This work on CFD modeling of mixed ventilation air with aerosol disinfectant flow can fill important gaps in the literature by providing insights into optimizing disinfection strategies in indoor spaces. It can also help develop guidelines for the effective use of aerosol disinfectants in conjunction with air conditioning systems.

Previous research studies have mainly focused at the methods to remove the indoor contaminants through the airflow. The success or failure of this goal in this type of designs depends entirely on the performance of the ventilation system. However, in the present study, establishing thermal comfort together with removing indoor contaminants, especially viruses by the help of the ventilation system and also disinfection of the interior space with the added sanitizer device were investigated. EUC parameter was also evaluated for the examined cases to improve the analysis. Therefore, the major purpose of the present research is to investigate the capability of the combined ventilation system and a sanitizer device in order to eliminate and remove the indoor contaminates mainly the viruses in health care facilities, SR in particular. Since medical treatments are directly dependent on HVAC systems, studying the HVAC systems is of high significance to reduce the spread of viruses in hospitals and health care facilities. A virus-infected patient may need surgery due to certain medical requirements. The presence of a virus-infected person in the SR can be very dangerous for the surgical staff. In addition to the use of personal protective equipment by the surgical staff, the proper design of the ventilation system plays a significantly role in eliminating the spread of virus contamination from the infected person and minimizes the risk of infection for the surgical staff. On the other hand, removing the pollution caused by virus in the SR keeps the health of the patient, the surgical staff and the success of the surgery. In the present research, by designing an air sanitization system, the air inside the SR is effectively disinfected for the staff and patients. This is critical in order to safeguard physicians, nurses, and other health care staff. The results of the current study could be considered by the HVAC engineers in order to control the spread of the viruses in SR and health care facilities.

2. Methodology

2.1. The Case Study

In this study, a SR in Chabahar Iranian surgery clinic, Chabahar, Iran (Case 1) was considered to examine the performance of the HVAC system. The interior view, dimensions and existing model of the SR are shown in Figure 1. Axes A, B, C, and D are related to the validation axes and axes E, F, G, and H are related to the mesh independence axes. The coordinate of the locations is tabulated in Table 1. The SR has four inlets on the ceiling and eight outlets at the corners of the room. An aerosol sanitizer device is modeled to disinfect the SR space throughout circulate in the SR space and eliminate virus contamination. Since droplets smaller than 5 μm were considered in this study, air was used as the sanitizer fluid. In addition to the existing case, two other different configurations with different inlet layouts were considered to investigate the effect of the ventilation system and it's mixing with aerosol sanitizer. Case 2 has two inlets, Case 3 has four inlets, and Case 4 has one inlet in the side walls, as illustrated in Figure 2. In all the cases, a patient with confirmed virus and a surgical bed are modeled to investigate the effect of ventilation on the room space. The dimensions of the surgical bed, aerosol sanitizer device and inlet diffusers and outlet vents and other equipment are tabulated in Table 2.

Fieldwork measurements were performed in three steps for all boundaries and validation locations, so an average of the three measured data was employed. Velocity and temperature at the input boundaries, temperature at the boundary of the room walls, temperature and velocity at the validation points were measured directly in the actual SR. A hot wire anemometer was used to determine field data. The instrument was calibrated using equipment previously calibrated to traceable international standards. The uncertainty of the measuring device is ± 2% for velocity, ± 0.4% for temperature, and ± 3% for humidity. Field measurements were conducted to determine the boundary conditions employed in the numerical study and also to validate the numerical model. The boundary conditions used for the CFD simulation in Case 1 have been determined from the field measurements. The data required for boundary conditions, including supply air temperature, velocity and air flow rate, were measured directly in the actual surgical room (case study in the present research). In order to eliminate any possible errors, the measurements were performed in three steps and a mean value was considered. Because the SR is located between adjacent rooms, a constant temperature boundary condition was considered for the walls. Table 3 shows the boundary conditions for the SR walls. The boundary condition of the manikin is defined as a surface temperature of 34 ^{o}C [27]. Other boundary conditions used in the design cases are tabulated in the Table 4.

Table 1. Coordinates of validation and mesh independent locations.

Location	Coordinate (m)	
	x	y
A	2.24	1.866
B	3.94	1.866
C	3.94	3.846
D	2.24	3.846
E	2.34	2.85
F	3.09	1.2
G	3.84	2.85
H	3.09	4.51

(a)

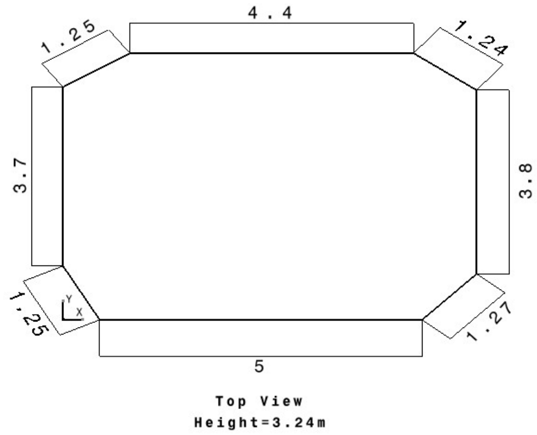

(b)

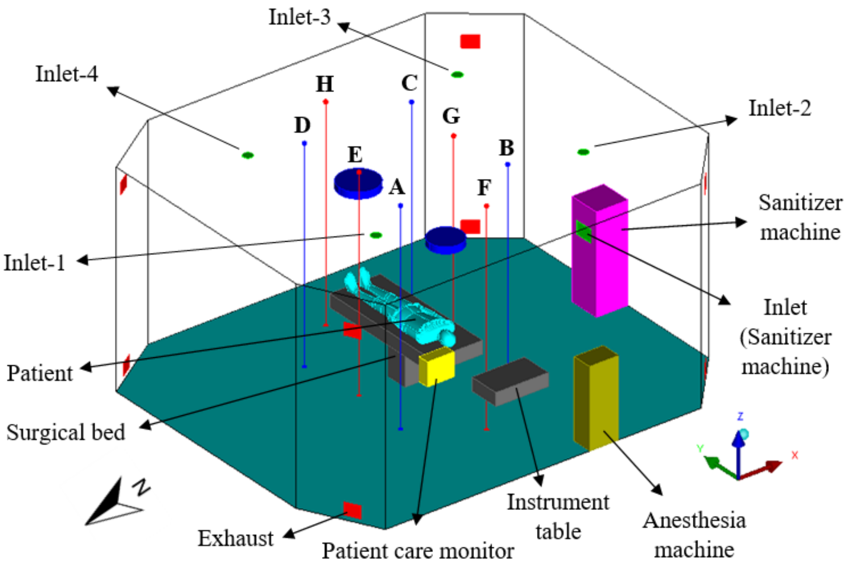

(c)

Figure 1. Existing SR (Case 1): (a) interior view of the Chabahar Iranian surgery clinic SR, (b) dimension (in meters), (c) the layout of the simulated SR.

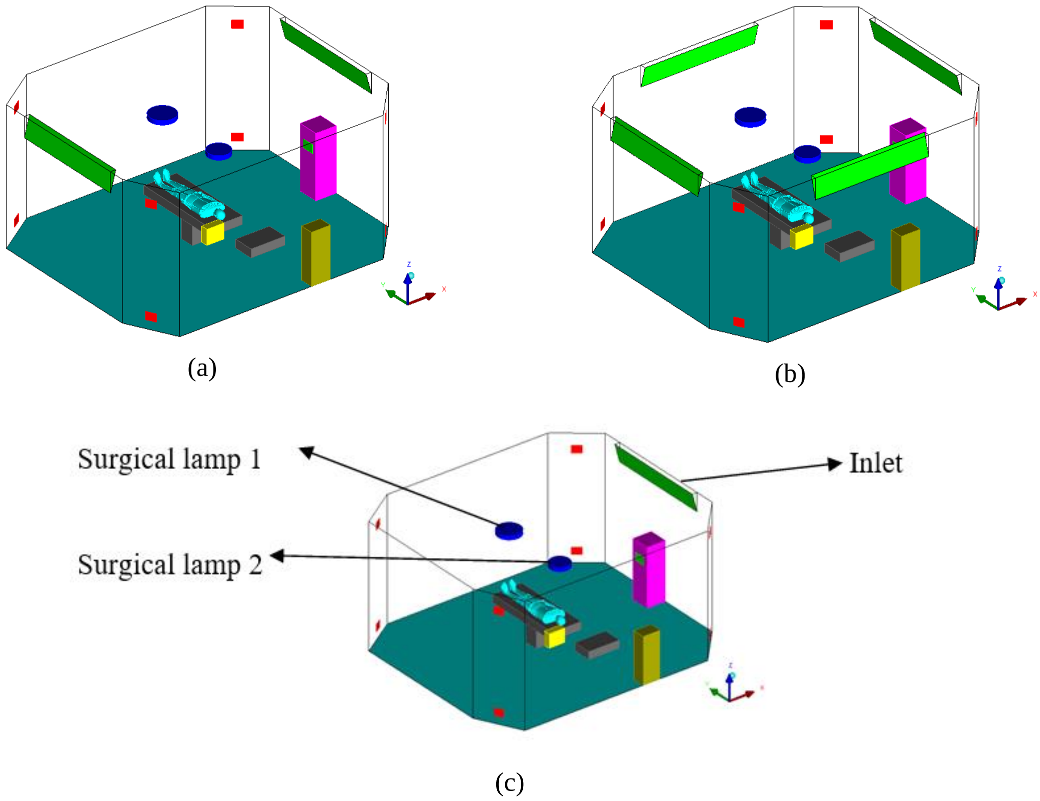

Figure 2. Design cases with the inlet diffusers' layout: (a) Case 2, (b) Case 3, (c) Case 4.

Table 2. Dimensions of the aerosol sanitizer device, surgical bed and inlet diffusers and outlet vents.

Item	Dimension (m)		
Anesthesia machine	0.46×0.315×1.22		
Surgical lamp 1	0.6 diameter × 0.1		
Surgical lamp 2	0.51 diameter × 0.1		
Instrument table	0.83 × 0.49 × 0.2		
Patient care monitor	0.42 × 0.17 × 0.36		
Sanitizer device	0.5×0.5×1.5		
Inlet of the sanitizer device	0.3×0.2		
Surgical bed	0.8×2.1×0.2		
The basis of surgical bed	0.305×0.35×0.685		
SR (for all cases)	Figure 1: (b)		
Inlet	Case 1	4 number	0.146 diameter
	Case 2	2 number	2.75×0.5
	Case 3	4 number	2.75×0.5
	Case 4	1 number	2.75×0.5
Exhaust	For all cases	8 number	0.235×0.185

Table 3. Boundary condition for the room walls.

Wall	N	S	E	W	C	F	N.E	N.W	S.E	S.W
Temperature (°C)	22.6	22.1	22.3	22.5	22.3	22.2	22.2	22.3	22.5	22.5

[N]Northern, [S] Southern, [E] Eastern, [W] Western, [C] Ceiling, [F] Floor, [N.E]Northeast, [N.W]Northwest, [S.E]Southeast, [S.W]Southwest.

Table 4. Boundary condition for CFD simulation.

Case	Boundary	Temperature (°C),	Velocity (m/s)	Heat source (W)
Case 1	Inlet-1	19.9	3.4	-
	Inlet-2	21.8	2.2	-
	Inlet-3	22.3	1.2	-
	Inlet-4	21.1	3.6	-
Case 2 & Case 3	Inlets	20	0.22	-
Case 4	Inlets	20	0.44	-
For all cases	Inlet-Sanitizer	24	0.2	-
For all cases	Manikin	34	-	-
For all cases	Anesthesia machine	-	-	200
For all cases	Surgical lamp 1	-	-	42
For all cases	Surgical lamp 1	-	-	42
For all cases	Patient care monitor	-	-	100

2.2. Numerical Method

A commercial CFD code was used to simulate the airflow in this study. This commercial CFD code was used to solve the governing equations of momentum, energy, pressure velocity coupling, turbulent kinetic energy, and turbulent dissipation rate. The choice of turbulent flow in simulating indoor airflow is one of the major challenges. Due to the scale and complexity of indoor airflow simulation, two-equation k-ε models are the most common models for a wide range of indoor airflow simulations [28]. The k-ε turbulence model has been widely used and proved in a wide range of indoor airflow simulations in recent decades. Among the k-ε turbulence models, the realizable k-ε model is a relatively recent development and is superior to the standard k-ε model [12, 29]. The realizable k-ε model has been proved to be suitable for the complex indoor environment's simulations [12, 13, 28, 30, 31]. The realizable k-ε model was chosen, because of its demonstrated ability to exactly predict the airflow in the indoor spaces [12, 32-34]. The turbulent flow properties in the near-wall regions were treated with enhanced wall treatment [12, 27, 28, 35]. The basic conservation equations for the steady state condition were solved using the finite volume method [12, 27, 28, 36, 37]. Pressure and velocity were coupled using the SIMPLE algorithm [3, 12, 27, 38-40].

The governing equations of momentum, energy, k, and ε were discretized by the second-order upwind scheme. As for the pressure equation, the "PRESTO!" scheme due to of its accuracy, was used in treating boundaries, because it accounts pressure gradients there [28, 35, 41]. The Boussinesq model is used for the buoyancy effect [27, 35, 36, 38, 42]. The convergence criteria for continuity, velocity, k and ε was considered as 1×10^{-3}, as well as 1×10^{-6} for the energy. The governing equations for continuity, momentum and energy are given below (Eqs. (1-4)) [43]:

$$\frac{\partial\rho}{\partial t}+\nabla.(\rho\vec{V})=0 \tag{1}$$

$$\frac{\partial(\rho u)}{\partial t}+\nabla.(\rho u\vec{V})=-\frac{\partial p}{\partial x}+\frac{\partial\tau_{xx}}{\partial x}+\frac{\partial\tau_{yx}}{\partial y}+\frac{\partial\tau_{zx}}{\partial z}+\rho f_x \tag{2}$$

$$\frac{\partial(\rho v)}{\partial t}+\nabla.(\rho v\vec{V})=-\frac{\partial p}{\partial y}+\frac{\partial\tau_{xy}}{\partial x}+\frac{\partial\tau_{yy}}{\partial y}+\frac{\partial\tau_{zy}}{\partial z}+\rho f_y \tag{3}$$

$$\frac{\partial(\rho w)}{\partial t}+\nabla.(\rho w\vec{V})=-\frac{\partial p}{\partial z}+\frac{\partial\tau_{xz}}{\partial x}+\frac{\partial\tau_{yz}}{\partial y}+\frac{\partial\tau_{zz}}{\partial z}+\rho f_z \tag{4}$$

$$\frac{\partial}{\partial t}(\rho E)+\nabla.(\vec{V}(\rho E+p))=\nabla.(k_{eff}\nabla T-\sum_j h_j\vec{J}_j+(\overline{\overline{\tau}}_{eff}.\vec{V})) \tag{5}$$

Where ρ is density (kg/m^3), $\vec{V}$ is velocity vector (m/s), *u,v,w, represent the c*omponents of velocity (m/s), P is static pressure (Pa), τ *is s*tress tensor (Pa), E is total energy (J), k_{eff} is effective conductivity (W/mK), T is temperature (^{o}C), and $\overline{\overline{\tau}}_{eff}$ is deviatoric stress tensor (Pa).

The turbulence kinetic energy, k, and its rate of dissipation, ε, for the realizable turbulent transport condition are obtained from the following equations [29, 44, 45]:

$$\frac{\partial}{\partial t}(\rho k)+\frac{\partial}{\partial x_j}(\rho k u_j)=\frac{\partial}{\partial x_j}\left[\left(\mu+\frac{\mu_t}{\sigma_k}\right)\frac{\partial k}{\partial x_j}\right]+G_k+G_b-\rho\varepsilon-Y_M+S_k \tag{6}$$

$$\frac{\partial}{\partial t}(\rho\varepsilon)+\frac{\partial}{\partial x_j}(\rho\varepsilon u_j)=\frac{\partial}{\partial x_j}\left[\left(\mu+\frac{\mu_t}{\sigma_\varepsilon}\right)\frac{\partial\varepsilon}{\partial x_j}\right]+\rho C_1S\varepsilon-\rho C_2\frac{\varepsilon^2}{k+\sqrt{\nu\varepsilon}}+C_{1\varepsilon}\frac{\varepsilon}{k}C_{3\varepsilon}G_b+S_\varepsilon \tag{7}$$

Where K is turbulence kinetic energy (m^2/s^2), μ_t is turbulence viscosity (kg/ms), σ_k is turbulent Prandtl number for k , σ_ε is turbulent Prandtl number for ε , G_b is generation of turbulence kinetic energy due to buoyancy (kg/ms^3), G_k is generation of turbulence kinetic energy due to the mean velocity gradients (kg/ms^3), ε is dissipation of turbulent kinetic energy (m^2/s^3), Y_M is contribution of the fluctuating dilation in compressible turbulence to the overall dissipation rate (kg/ms^3), S_k,S_ε are source terms, C_1, C_2,$C_{1\varepsilon}$, $C_{3\varepsilon}$ are model constants in the term of the k and ε model, and ν is kinematic viscosity (m^2/s).

To make the physical description more manageable, it is necessary to simplify certain aspects and make several assumptions to facilitate calculations. The SR space is simulated in 3D, the air flow is turbulent, the fluid is air, there are no chemical reactions between the components of the fluid, the walls of the room are at constant temperature, the temperature and velocity at the inlet boundaries of Case 1 are determined from field measurements, the patient's body surface temperature is considered to be a constant temperature, and the heat sources include surgical lamps, anesthesia machine, and patient care monitor.

An unstructured mesh (tetrahedral) was used for the SR space (see Figure 3). 10 prism layers was located on the surfaces with an initial height of 0.2 mm and growth rate of 1.13 in each cell layer, which resulting in y^+ values lower than three (y^+ <3) on the manikin surfaces. A mesh independence test (Figure 4) was conducted using four different mesh resolutions with the cell numbers of 1154836, 1399679, 1826782, and 2192142. No significant differences in the temperature field were found between 1826782 and 2192142 cells. Therefore, the mesh with a total number of about 2 million cells was adopted.

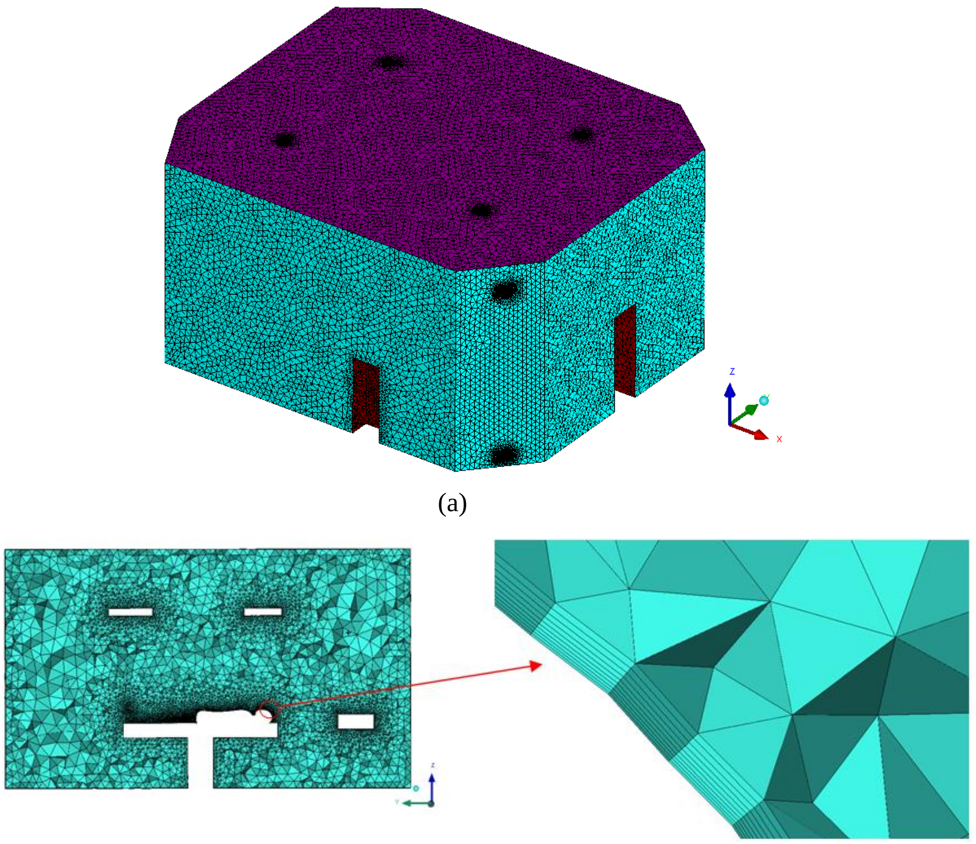

(a)

(b)

Figure 3. The grid mesh of the CFD simulations: (a) mesh for the room model, (b) sectional view of the mesh for computational domain and detailed mesh structure for the region near the thermal manikin.

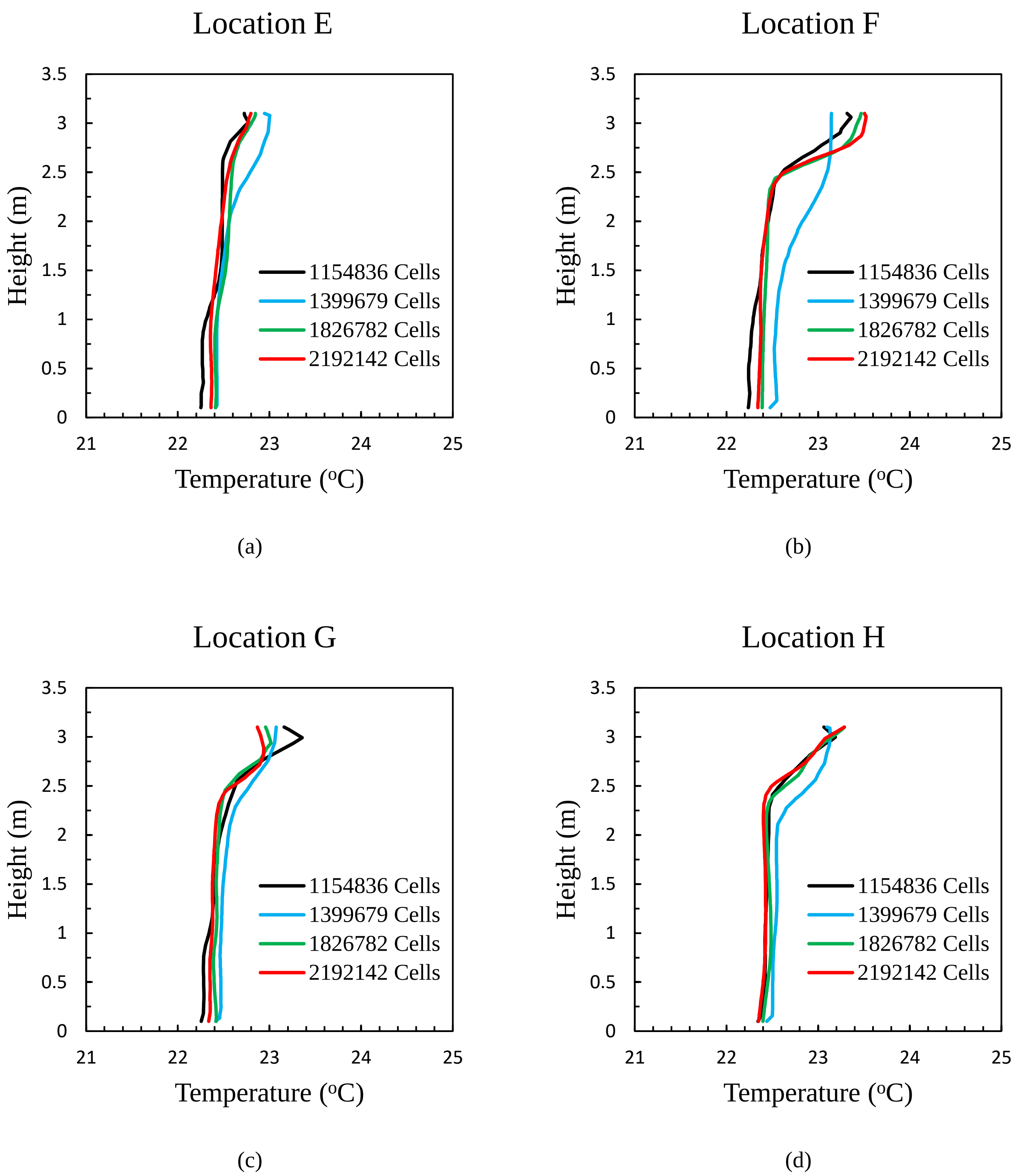

Figure 4. Temperature variation at different mesh numbers: (a) location E, (b) location F, (c) location G, (d) location H.

3. Results and Discussions

The present study investigated the effect of aerosol sanitizer system added to a SR space to safeguard the lives of health care staffs in the SR room. Since patients with viral infections may require surgical procedures, so this study has focused on the removal and disinfection of the indoor SR. In the present research, the possibility of improving the performance of the operating ventilation system by mixing the conditioned air (supply air) with an aerosol sanitizer outlet flow was investigated.

The experimental method used to validate the numerical model was based on the field measurements. Therefore, to validate the numerical model, the spot measured data were recorded in four locations in the surgical room and compared with the simulation data. For this purpose, a hot wire anemometer was used. To eliminate any possible errors, the field measurements were performed in three steps for each location, which included a total of 40 measuring points. The mean values were considered. To validate the CFD method, the simulation results were compared with the field measurements. The validation of the CFD method was based on the values of the existing case (i.e. Case 1). Validation was performed based on the velocity and temperature values in four locations A, B, C, and D (see Figure 1). Figure 5 and Figure 6 shows a comparison between field measurements and simulation values. As shown in Figure 5, the maximum deviation for velocity between the simulations and field measurements is 8.81%, moreover as shown in Figure 6 the present simulation predicts the fieldwork measurement data with appropriate accuracy in all cases, so that the maximum deviation for temperature was 4.78%. A statistical analysis of the validation data was performed using the mean absolute error between the measured and simulated temperature values in axes A to D (see Table 5 to 8). These metrics confirm that the CFD model provides reliable results within an acceptable margin of error.

Table 5. Fieldwork measurement and simulation data on the A axis

Height (m)	Experimental data (T °C)	Simulation data (T °C)	Error (%)
0.1	22.5	21.7	3.56
0.5	22.7	21.8	3.96
1	22.7	21.8	3.96
1.15	22.7	21.8	3.96
1.2	22.7	21.8	3.96
1.5	22.8	21.9	3.95
1.7	22.8	21.9	3.95
2	22.8	21.9	3.95
2.5	22.7	21.9	3.52
3	22.5	22.2	1.33

Table 6. Fieldwork measurement and simulation data on the B axis

Height (m)	Experimental data (T °C)	Simulation data (T °C)	Error (%)
0.1	22.3	21.8	2.24
0.5	22.4	21.8	2.68
1	22.6	21.8	3.54
1.15	22.7	21.8	3.96
1.2	22.7	21.8	3.96
1.5	22.8	21.8	4.39
1.7	22.8	21.8	4.38
2	22.7	21.9	3.52
2.5	22.5	21.9	2.67
3	22.2	22	0.90

Table 7. Fieldwork measurement and simulation data on the C axis

Height (m)	Experimental data (T °C)	Simulation data (T °C)	Error (%)
0.1	22.2	21.8	1.80
0.5	22.2	21.8	1.80
1	22.3	21.9	1.79
1.15	22.4	21.9	2.23
1.2	22.4	21.9	2.23
1.5	22.5	21.9	2.67
1.7	22.5	21.9	2.67
2	22.6	21.9	3.10
2.5	22.5	21.9	2.67
3	22.1	22	0.45

Table 8. Fieldwork measurement and simulation data on the D axis

Height (m)	Experimental data (T ºC)	Simulation data (T ºC)	Error (%)
0.1	22.4	21.7	3.12
0.5	22.6	21.8	3.54
1	22.7	21.8	3.96
1.15	22.8	21.8	4.39
1.2	22.9	21.9	4.37
1.5	22.9	21.9	4.37
1.7	23	21.9	4.78
2	23	21.9	4.78
2.5	22.7	21.9	3.52
3	22.5	22	2.22

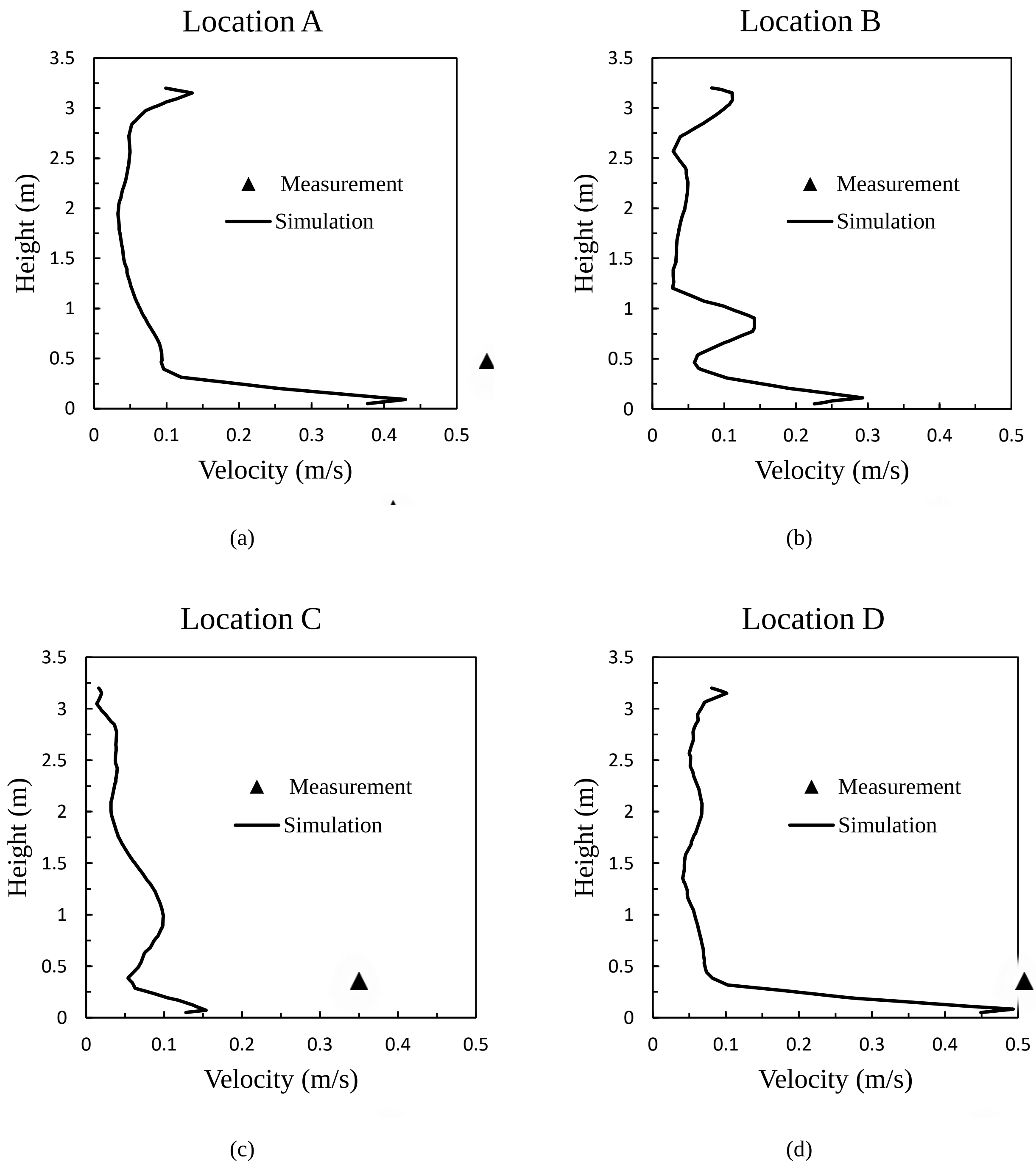

Figure 5. Comparison of the simulation and field measurements: (a) location A, (b) location B, (c) location C, (d) location D.

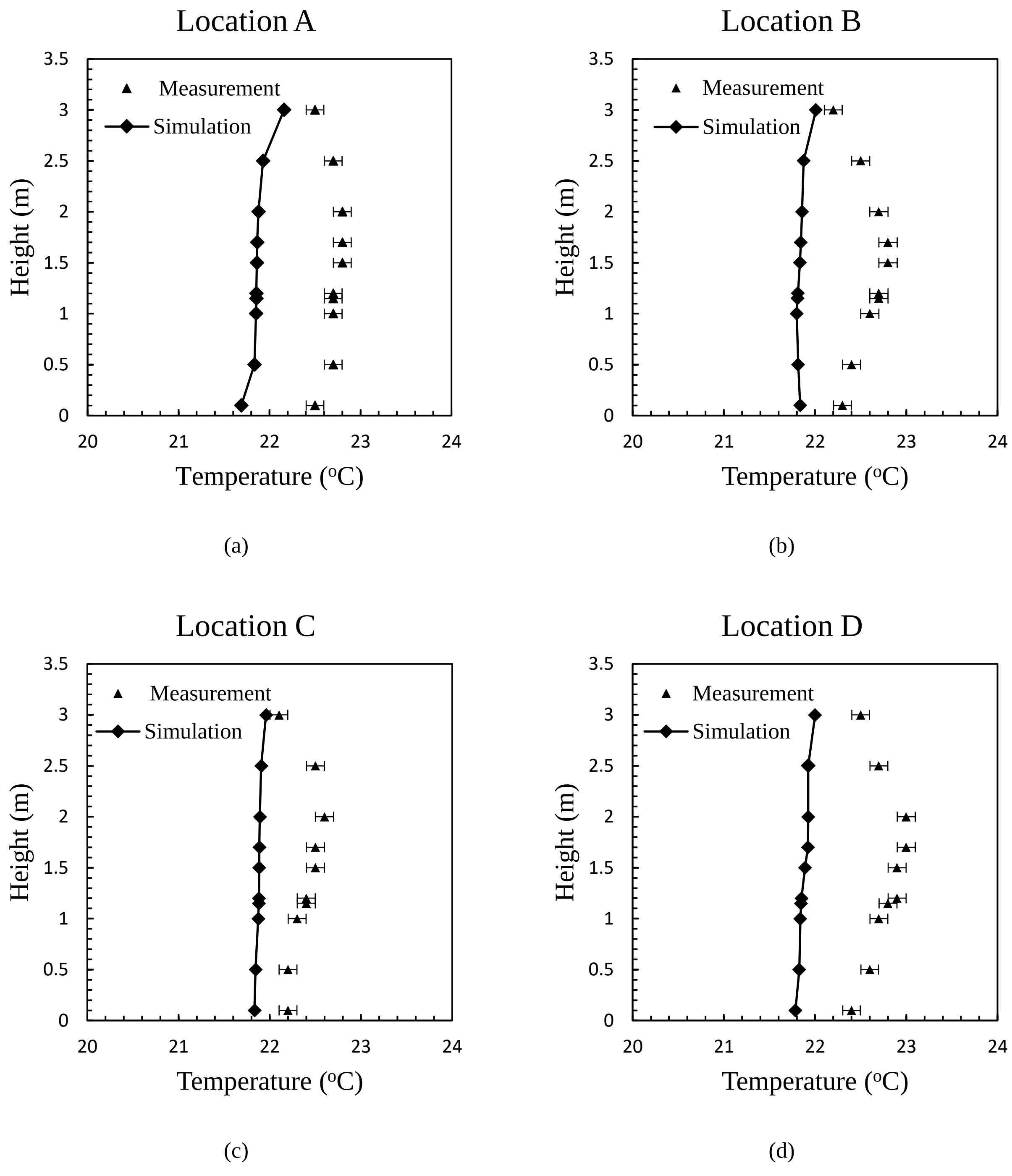

Figure 6. Comparison of the simulation and fieldwork measurement values: (a) location A, (b) location B, (c) location C, (d) location D.

3.1. Air Distribution Patterns

Figures 7 and 8 (top view) shows the path lines of inlet air and aerosol sanitizer flow. In Case 1, the airflow falls downwards and subsequently spreads toward the walls after striking the floor. The outlet flow from the aerosol sanitizer in this model, first moves upwards and a part of the flow changes downwards to the floor after reaching the inlet air. In this model, the aerosol sanitizer system has less diffusion into the surgical area (SA) where the patient with infected virus is located. In this case, due to the upward flow of aerosol sanitizer, it does not have a direct effect on the SA. In Case 2, the aerosol sanitizer flow, although penetrating the SA, is not able to penetrate all the space of the room, especially the corners of the room; therefore, this causes SR contaminants, especially the virus, to spread from the patient with infected virus, accumulate in these areas and increase the risk of infection for the surgical staff. The inlet airflow in Case 3 creates a barrier to the aerosol sanitizer system. In this case, the aerosol sanitizer flow is not capable of entering the SA and SR space and moves directly to the outlet vents. The ventilation system in this case is not effective, since the flow of aerosol sanitizer is prevented into the room space and goes directly to the outlet vents. In Case 4, the inlet airflow, after mixing with the aerosol sanitizer flow, spreads directly to the SA. In this case, due to the direct entry of aerosol sanitizer into the SA, it is a suitable system for disinfecting the SR space, especially the SA. Therefore, the aerosol sanitizer mixes well with the inlet airflow and disinfects the entire SR space. Therefore, it is expected to inactivate viral contaminants effectively.

Figure 9 shows the velocity vector for different cases on plane Y = 2.856 m. The vectors are based on the velocity magnitude. The direction of the sanitizer flow vectors in Case 1 is upwards. In this case, the sanitizer flow moves upwards along with the inlet air flow, and this makes the SA not being disinfected quickly and effectively. In Case 2 and Case 3, due to the air curtain created by the inlet air, the sanitizer flow is trapped outside the SA inside large vortices and does not flow to the SA and other parts of the SR. This causes the sanitizer flow to circulate only outside the SA and not enter into the interior of the room. In these cases, the sanitizer flow is discharged through the outlet vents without creating effective disinfection. In Case 4, the inlet air flow and the sanitizer mix quickly. In this case, the sanitizer flow moves to the SA along with the inlet air flow and disinfects the indoor space by circulating in the room space. It is expected that the SR air will be effectively disinfected in Case 4, and patients and surgical staff could be protected from the risk of infection. The air flow velocity in Case 1 around the patient's body is less than 0.03 m/s and for Case 2 and Case 3 it is about 0.1 m/s. The low air velocity in these cases creates a static area around the patient's body and prevents good mixing of air with disinfectant in the SA, which in turn increases contamination in the SA. In model 4, due to the creation of an appropriate air flow velocity in the SA (more than 0.15 m/s), by creating a dynamic area, it helps to properly mix air with disinfectant, and this creates a safe area for the patient.

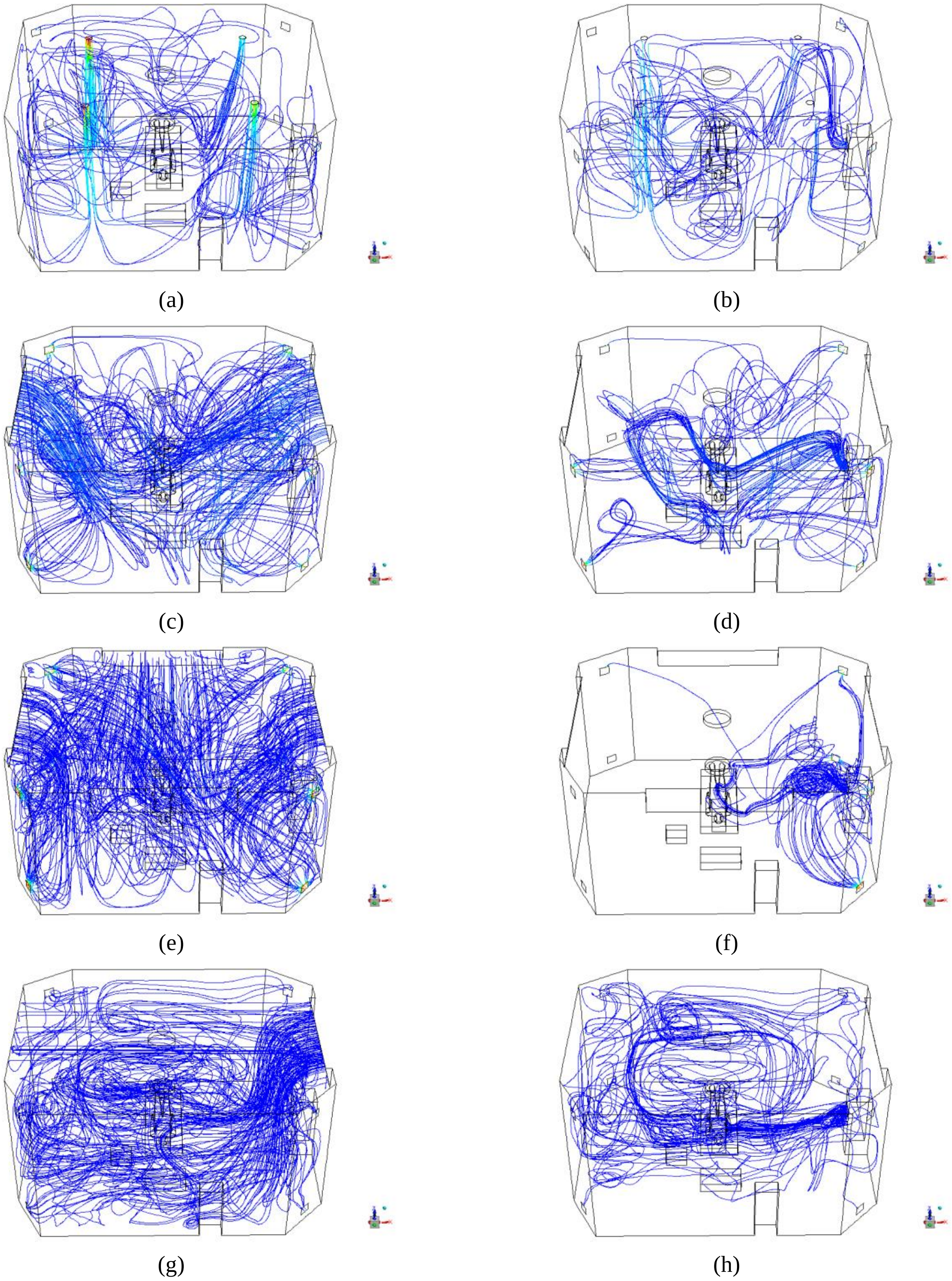

(a) (b) (c) (d) (e) (f) (g) (h)

Figure 7. Path line for inlet diffusers and inlet of sanitizer: (a) Case 1 for inlet diffusers, (b) Case 1 for inlet of sanitizer, (c) Case 2 for inlet diffusers, (d) Case 2 for inlet of sanitizer, (e) Case 3 for inlet diffusers, (f) Case 3 for inlet of sanitizer, (g) Case 4 for inlet diffusers, (h) Case 4 for inlet of sanitizer.

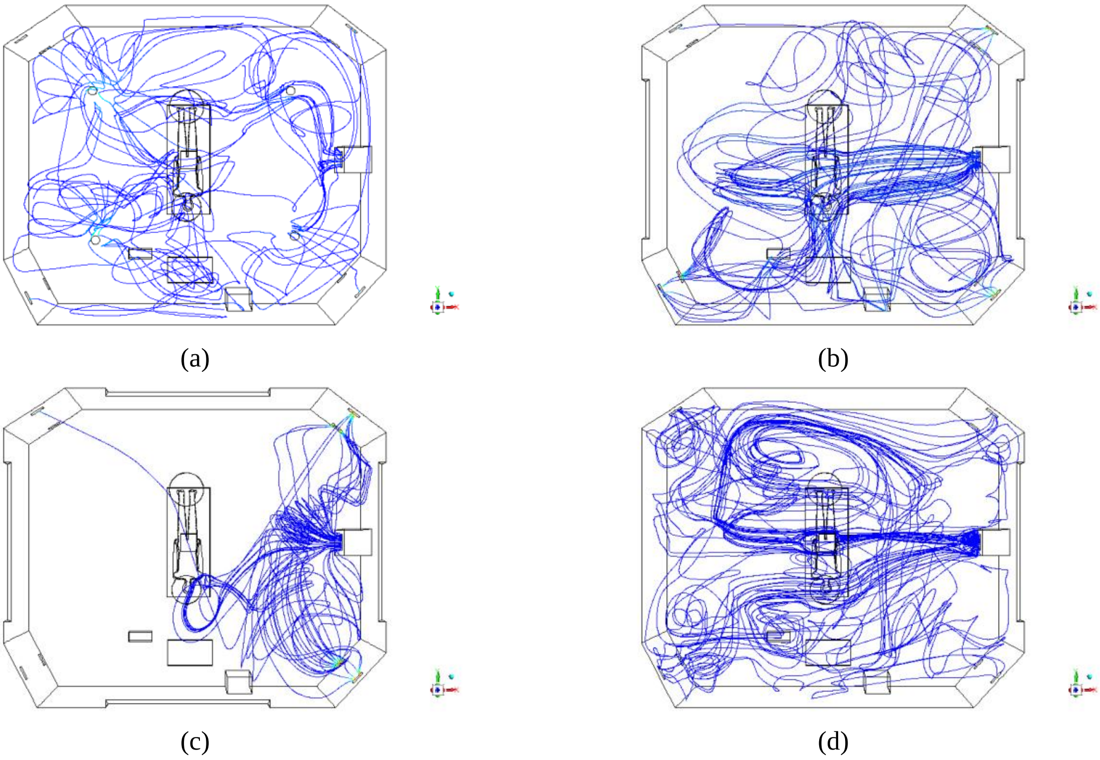

Figure 8. Path line for inlet of sanitizer (top view): (a) Case 1, (b) Case 2, (c) Case 3, (d) Case 4.

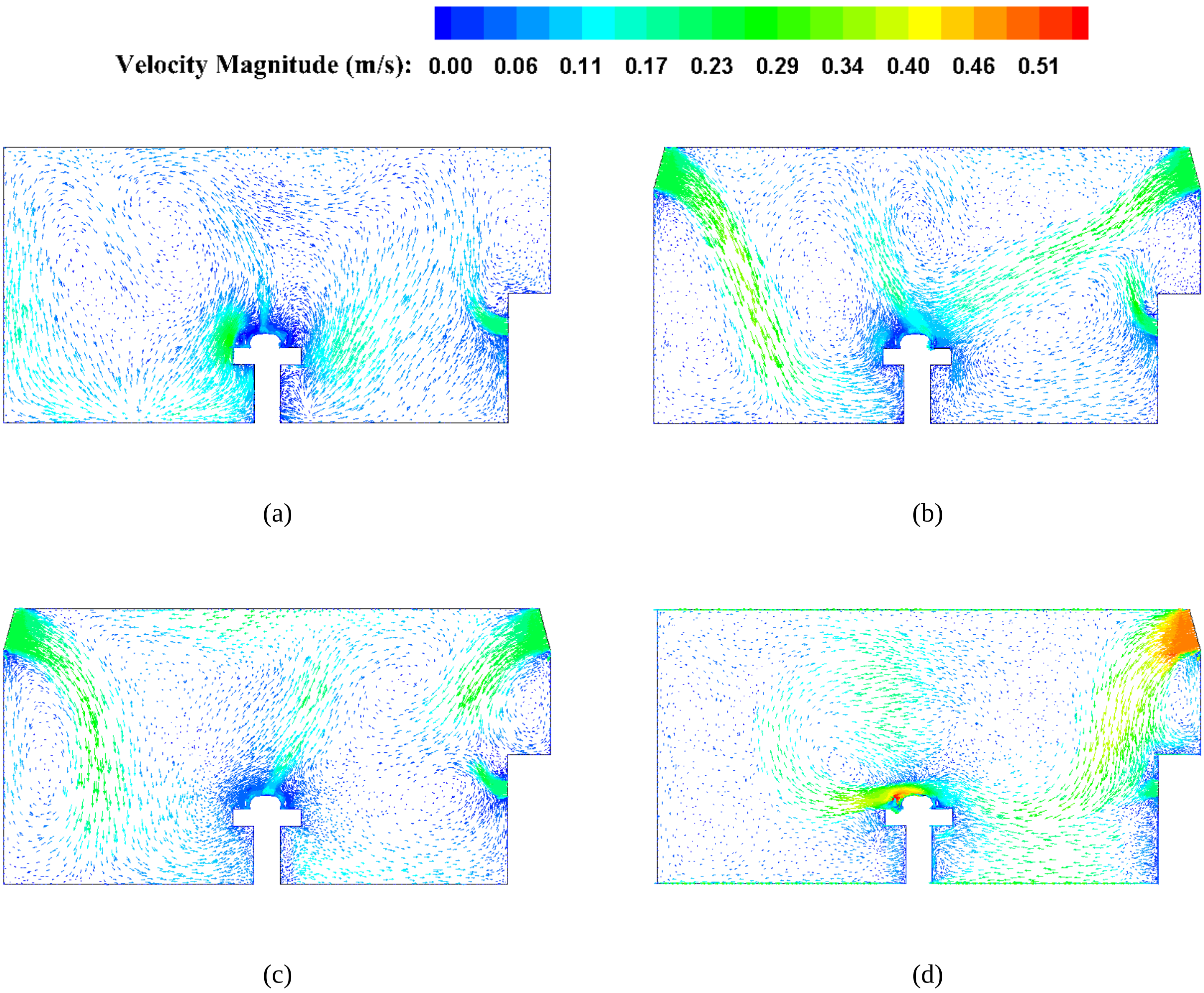

Figure 9. Velocity vectors on plane Y = 2.856 m: (a) Case 1, (b) Case 2, (c) Case 3, (d) Case 4.

Figure 10 illustrates the temperature distribution on plane Y = 2.856 m. It is clear from this figure that the sanitizer is released at a higher temperature by the sanitizing system, which the cool air from the inlet diffusers mixes with it. In Case 4, due to the temperature and velocity gradient between the sanitizing device's flow and the air inlet, a better mixing is done than the other cases. In this case, due to the effect of temperature and velocity gradient maintained by the sanitizing system, the cool air coming from the inlet diffuser has an asymmetric pattern, which helps to properly mix the inlet air and sanitizer flow. The ASHRAE [46, 47] standard recommends a temperature of 20 °C to 24 °C for the SR. In Case 1, due to poor ventilation, the patient experiences a temperature of approximately above 24 °C, which is outside the range recommended by the ASHRAE standard. Cases 2 to 4 create the suitable temperature distribution for the SR space. The temperature in these cases is between 20 °C to 24 °C, which is within the standard recommended range. In these cases, the patient experiences a comfortable temperature according to the ASHRAE standard.

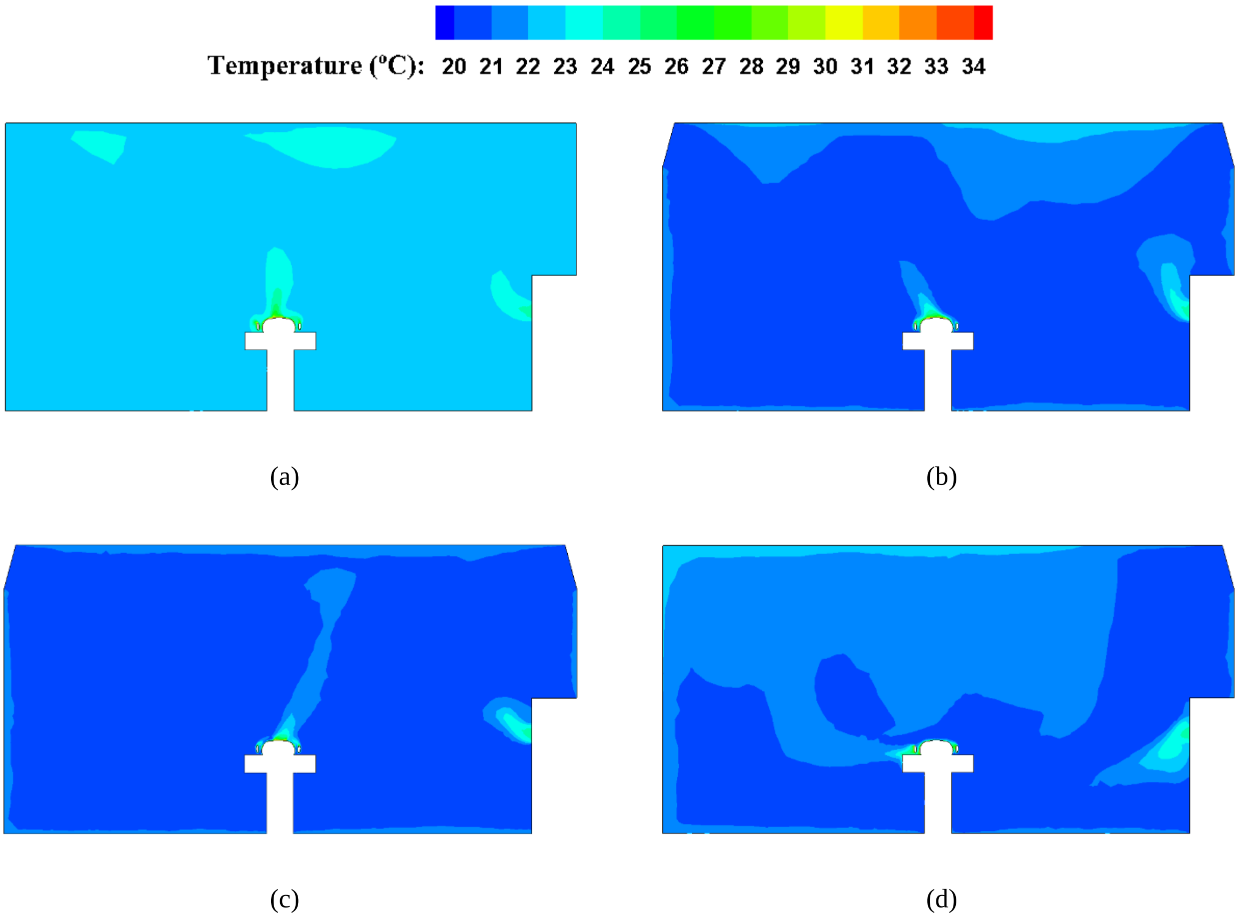

Figure 10. Temperature distribution on plane Y = 2.856 m: (a) Case 1, (b) Case 2, (c) Case 3, (d) Case 4.

Figure 11 shows the turbulent intensity contour for Case 4. As shown in Figure 11, the turbulent intensity near the walls of the SR (about 12%) and the SA (about 5%) is higher than other areas, and this ensures more circulating and mixing of aerosol sanitizer in these areas. In other words, in the SA and the corner of the walls, where there is a high probability of deposition of particles contaminated with virus, the aerosol sanitizer device is able to disperse aerosol sanitizer to these areas. Hence, by being distributed in these areas, the aerosol sanitizer has the capability to eliminate the viruses and thus ensures the health of the patient and the surgical staff.

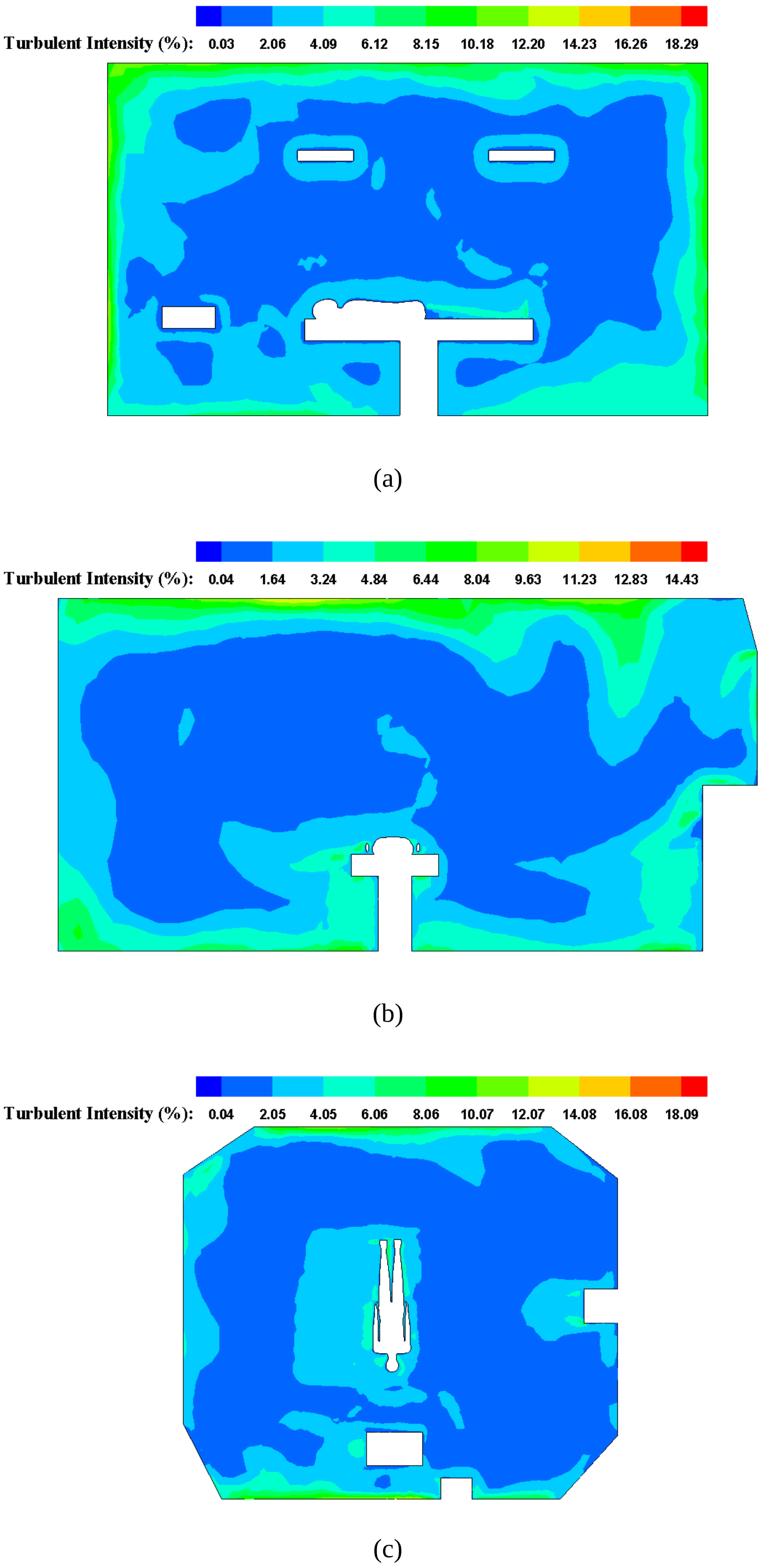

Figure 11. Turbulent intensity for Case 4: (a) X=3.06 m, (b) Y = 2.856 m, (c) Z=0.93 m.

3.2. Thermal Comfort Analysis

Thermal comfort is affected by many factors, such as temperature and dynamic airflow [36, 48, 49]. The assessment of thermal comfort in indoor environment is usually determined by predicted mean vote (PMV) and predicted percentage dissatisfied (PPD). This model was developed by Fanger [50] using heat balance equations and empirical studies to define comfort. The thermal comfort assessment was performed using the Fanger model as bellow [36, 50, 51]:

$$PMV = \left(0.303e^{-0.036M} + 0.028\right) \times \left\{ \begin{array}{l} (M-W) - 3.05\times10^{-3}\times[5733 - 7(M-W) - P_a] \\ -0.42[(M-W) - 58.15] - 1.73\times10^{-5}M(5867 - P_a) \\ -0.0014M\times[34 - t_a] + 3.96\times10^{-8} f_{cl}\left[(t_r+273)^4 - (t_{cl}+273)^4\right] \\ + f_{cl}h_c(t_a - t_{cl}) \end{array} \right\} \tag{8}$$

Where:

$$t_{cl} = t_{s,mean} - I_{cl}\left\{3.96\times10^{-8} f_{cl}\times\left[(t_{cl}+273)^4 - (t_r+273)^4\right] + f_{cl}h_c(t_{cl} - t_a)\right\} \tag{9}$$

$$h_c = \begin{cases} 2.38(t_{cl}-t_a)^{0.25} & 2.38(t_{cl}-t_a)^{0.25} > 12.1\sqrt{V_a} \\ 12.1\sqrt{V_a} & 2.38(t_{cl}-t_a)^{0.25} < 12.1\sqrt{V_a} \end{cases} \tag{10}$$

$$f_{cl} = \begin{cases} 1.0 + 0.2I_{cl} & I_{cl} < 0.5clo \\ 1.05 + 0.1I_{cl} & I_{cl} > 0.5clo \end{cases} \tag{11}$$

$$PPD = 100 - 95\times e^{-\left(0.03353\times PMV^4 + 0.2179\times PMV^2\right)} \tag{12}$$

Where M is metabolic rate (W/m^2), W is output working power of human (W), P_a is water vapor partial pressure (Pa), t_a is air temperature (^{o}C), f_{cl} is clothing surface area factor (m2K/W), t_r is mean radiant temperature (^{o}C), t_{cl} is clothing surface temperature (^{o}C), h_c is convective heat transfer coefficient (W/m^{2}K), $t_{s,mean}$ is skin temperature (^{o}C), I_{cl} is thermo-resistance of clothes (m^{2}K/W), and V_a, is output working power of human (W).

ISO 7730 [52] recommends acceptable thermal comfort for indoor environment at -0.5 <PMV <+0.5. Table 9 shows the PMV values in the four locations E, F, G, and H, where the surgical staff is located. PMV values are within the standard recommended range and at neutral condition. Therefore, in the interior of the SR, the thermal conditions are completely suitable for the occupants. In almost all the locations, the PMV values in Case 1 have the maximum difference from zero, the maximum difference of PMV values from zero for Case 1 is 0.36 and while Cases 2, 3, and 4 have the minimum difference from zero. The maximum difference of PMV values from zero for Case 2 is 0.24, for Case 3 is 0.22, for Case 4 is 0.29. which means that the thermal conditions are quite suitable for Cases 2, 3, and 4.

Table 9. PMV values at different location in SR.

Height (m)	PMV															
	Location E				Location F				Location G				Location H			
	Case 1	Case 2	Case 3	Case 4	Case 1	Case 2	Case 3	Case 4	Case 1	Case 2	Case 3	Case 4	Case 1	Case 2	Case 3	Case 4
0.2	0.18	-0.05	-0.06	0	0.16	-0.1	-0.11	-0.04	0.4	0.2	0.11	0.1	0.21	-0.02	0.03	-0.04
0.4	0.19	-0.05	-0.05	0	0.2	-0.1	-0.07	-0.04	0.38	0.2	0.13	0.15	0.25	-0.01	0	0
0.6	0.19	-0.03	-0.04	0.01	0.22	-0.09	0	-0.06	0.36	0.22	0.16	0.18	0.31	0	-0.01	0.01
0.8	0.19	0.01	-0.04	-0.01	0.28	-0.1	0	-0.08	0.36	0.22	0.17	0.14	0.31	0.01	0	0.02
1.0	0.2	0.04	-0.02	-0.1	0.26	-0.12	-0.01	-0.05	0.37	0.19	0.19	0.15	0.29	0	0.02	-0.01
1.2	0.24	0.05	0	0.02	0.25	-0.12	-0.02	-0.05	0.4	0.15	0.21	0.2	0.28	-0.01	0.02	0.02
1.4	0.28	0.07	0.04	0.06	0.24	-0.11	-0.02	0.02	0.41	0.13	0.22	0.24	0.29	0	0.01	0.03
1.6	0.31	0.08	0.07	0.02	0.24	-0.08	-0.02	0.05	0.43	0.13	0.21	0.28	0.29	0.03	-0.02	0.01
1.8	0.32	0.06	0.06	0.01	0.24	-0.05	-0.03	0.05	0.44	0.16	0.2	0.28	0.3	0.07	-0.08	0.04
2.0	0.32	0.04	0.04	0.02	0.24	-0.02	-0.03	0.04	0.45	0.24	0.19	0.29	0.3	0.1	-0.17	0.04

Figure 12 demonstrates the PPD values for the four design cases. It was found that the PPD values for all the cases are less than 10% and within the recommended range of ISO 7730 (PPD recommendation value is ≤ 10%). The PPD values in Case 1 is higher than other models, as shown in Figure 12. As explained before, Case 4 has an acceptable performance in terms of indoor space disinfection and elimination of indoor contaminants, especially the virus which is spread from the patient. In addition, it was also revealed that the PPD values in Case 4 are less than the existing case (Case 1) and this proves people's satisfaction with the thermal conditions in the proposed model, namely Case 4 (see Figure 12).

3.3. Energy analysis

The energy utilization efficiency of air distribution system can be shown by the temperature difference between the air inside and outside the occupied area [53]. To evaluate the effectiveness of energy utilization of air distribution the EUC parameter is used [36, 53] as the following equation:

$$EUC = \frac{t_{uz} - t_s}{t_{oz} - t_s} \times 100 \tag{13}$$

Table 10 shows EUC values for design cases. EUC values are usually less than 100% for mixing ventilation and more than 100% for displacement ventilation as tabulated in Table 10. Energy savings depend on the EUC coefficient, so the greater the EUC, the greater the energy savings. Due to the fact that heat in the simulated space is generated by the manikin model as well as surgical equipment such as medical lamps, patient care monitor and anesthesia machine; therefore, the air temperature in the occupied area is higher than the unoccupied area. EUC analysis for different cases proves that Case 4 has the highest EUC value (about 95%) and Case 3 has the lowest EUC value (about 73%), so this case has the highest energy saving potential.

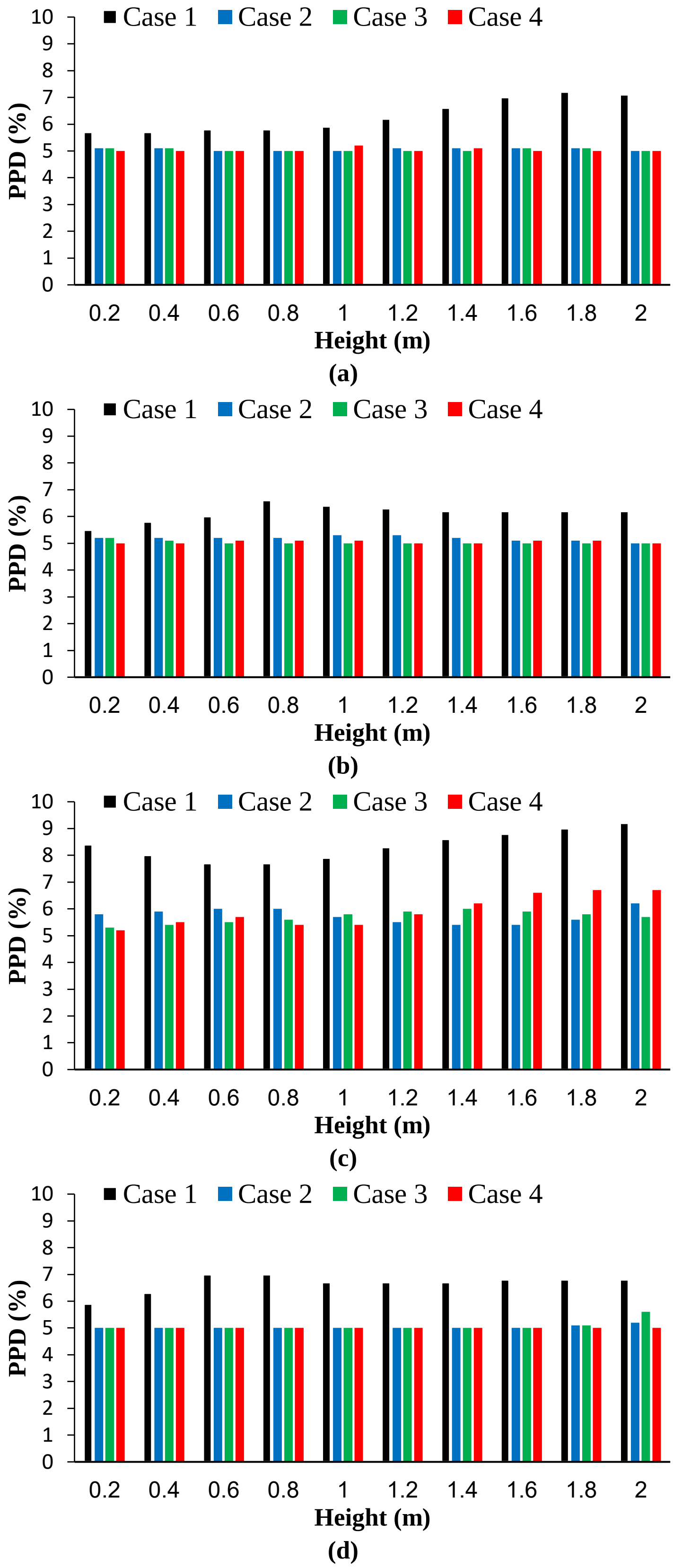

Figure 12. Comparison of PPD values: (a) location E, (b) location F, (c) location G, (d) location H.

Table 10. The EUC values of cases.

Cases	t_s (ºC)	t_{uz} (ºC)	t_{oz} (ºC)	EUC (%)
Case 1	21.28	22.48	22.77	80.54
Case 2	20	20.57	20.73	78.08
Case 3	20	20.43	20.59	72.88
Case 4	20	20.81	20.85	95.29

4. Conclusions

The present study investigated the possibility of improving the performance of the operating ventilation system by mixing the conditioned air (supply air) with an aerosol sanitizer outlet flow to eliminate viruses in a SR. The flow patterns for inlet air and aerosol sanitizer were analyzed for a total of four cases with different inlet diffusers.

The results showed that the existing case (Case 1) is not able to create suitable conditions for disinfecting the indoor air. Cases 2 and 3, which have two and four inlet diffusers in the side walls, respectively, prevent the entry of aerosol sanitizer flow into the SA and the room space by creating a barrier of air curtain. These models carry the aerosol sanitizer flow directly to the outlet vents without disinfecting the interior; therefore, they are not suitable systems for mixing aerosol sanitizer with inlet air. Examination of the flow pattern for Case 4 showed a suitable pattern for mixing aerosol sanitizer with inlet air. In Case 4, the aerosol sanitizer flow flows into the SA and the room space after mixing with the inlet air. Case 4 has the capability to circulate the aerosol sanitizer flow to every corner of the room. Therefore, the viruses are expected to be eliminated, and patients and surgical staff could be protected from the risk of viruses. In terms of thermal comfort point of view, Case 4 also established suitable conditions for the patient and indoor space. Energy analysis was also conducted for the cases employing the ECU parameter. It was revealed that Case 4 has the highest EUC value. Therefore Case 4 has the highest energy saving potential.

Acknowledgements

The authors would like to express their gratitude to Chabahar University of Maritime and Marine Sciences and Chabahar Iranian Surgery Clinic for their cooperation during the research.

References

[1] Ding, J., C.W. Yu, and S.-J. Cao, *HVAC systems for environmental control to minimize the COVID-19 infection.* Indoor and Built Environment, 2020. 29(9): p. 1195-1201.

[2] Aganovic, A. and G. Cao, *Evaluation of airborne contaminant exposure in a single-bed isolation ward equipped with a protected occupied zone ventilation system.* Indoor and Built Environment, 2019. 28(8): p. 1092-1103.

[3] Borro, L., et al., *The role of air conditioning in the diffusion of Sars-CoV-2 in indoor environments: A first computational fluid dynamic model, based on investigations performed at the Vatican State Children's hospital.* Environmental Research, 2021. 193: p. 110343.

[4] Rolloos, M., *HVAC systems and indoor air quality.* Indoor and Built Environment, 1993. 2(4): p. 204-212.

[5] Zhang, Y., et al., *Comparative research on the air pollutant prevention and thermal comfort for different types of ventilation.* Indoor and Built Environment, 2020: p. 1420326X20925521.

[6] Hwang, R.-L., et al., *Patient thermal comfort requirement for hospital environments in Taiwan.* Building and environment, 2007. 42(8): p. 2980-2987.

[7] Memarzadeh, F. and A. Manning, *Thermal comfort, uniformity, and ventilation effectiveness in patient rooms: performance assessment using ventilation indices.* Transactions-American Society of Heating Refrigerating and Air Conditioning Engineers, 2000. 106(2): p. 748-761.

[8] Verheyen, J., et al., *Thermal comfort of patients: Objective and subjective measurements in patient rooms of a Belgian healthcare facility.* Building and Environment, 2011. 46(5): p. 1195-1204.

[9] Van Gaever, R., et al., *Thermal comfort of the surgical staff in the operating room.* Building and Environment, 2014. 81: p. 37-41.

[10] Loomans, M., et al., *Alternative ventilation system for operating theaters: Parameter study and full-scale assessment of the performance of a local ventilation system.* Building and Environment, 2016. 102: p. 26-38.

[11] Chow, T.-T. and J. Wang, *Dynamic simulation on impact of surgeon bending movement on bacteria-carrying particles distribution in operating theatre.* Building and environment, 2012. 57: p. 68-80.

[12] Sadrizadeh, S., et al., *Numerical simulation of the impact of surgeon posture on airborne particle distribution in a turbulent mixing operating theatre.* Building and Environment, 2016. 110: p. 140-147.

[13] Romano, F., et al., *Numerical and experimental analysis of airborne particles control in an operating theater.* Building and Environment, 2015. 89: p. 369-379.

[14] Gholami Motlagh, V. and M. Ahmadzadehtalatapeh, *Optimization of Air Distribution Patterns by Arrangements of Air Inlets and Outlets: Case Study of an Operating Room.* Journal of Applied and Computational Mechanics, 2022. 8(3): p. 809-830.

[15] Gholami Motlagh, V., M. Ahmadzadehtalatapeh, and O. Mohammadi, *Effect of turbulent and laminar flow mechanisms on airflow patterns and CO2 distribution in an operating room: a numerical analysis.* Scientia Iranica, 2022. 30(3): p. 1008-1026.

[16] Liu, Z., et al., *Effect of a circulating nurse walking on airflow and bacteria-carrying particles in the operating room: An experimental and numerical study.* Building and Environment, 2020. 186: p. 107315.

[17] Zhang, Y., et al., *The impact of air change rate on the air quality of surgical microenvironment in an operating room with mixing ventilation.* Journal of Building Engineering, 2020. 32: p. 101770.

[18] Ho, S.H., L. Rosario, and M.M. Rahman, *Three-dimensional analysis for hospital operating room thermal comfort and contaminant removal.* Applied Thermal Engineering, 2009. 29(10): p. 2080-2092.

[19] Berlanga, F., et al., *Experimental assessment of different mixing air ventilation systems on ventilation performance and exposure to exhaled contaminants in hospital rooms.* Energy and Buildings, 2018. 177: p. 207-219.

[20] Bhattacharyya, S., et al., *A novel CFD analysis to minimize the spread of COVID-19 virus in hospital isolation room.* Chaos, Solitons & Fractals, 2020. 139: p. 110294.

[21] Ren, J., et al., *Numerical Study of Three Ventilation Strategies in a prefabricated COVID-19 inpatient ward.* Building and Environment, 2021. 188: p. 107467.

[22] Shao, S., et al., *Risk assessment of airborne transmission of COVID-19 by asymptomatic individuals under different practical settings.* Journal of aerosol science, 2021. 151: p. 105661.

[23] Dbouk, T. and D. Drikakis, *On coughing and airborne droplet transmission to humans.* Physics of Fluids, 2020. 32(5): p. 053310.

[24] Li, Y., et al., *Probable airborne transmission of SARS-CoV-2 in a poorly ventilated restaurant.* Building and Environment, 2021: p. 107788.

[25] Vuorinen, V., et al., *Modelling aerosol transport and virus exposure with numerical simulations in relation to SARS-CoV-2 transmission by inhalation indoors.* Safety Science, 2020. 130: p. 104866.

[26] Peng, S., Q. Chen, and E. Liu, *The role of computational fluid dynamics tools on investigation of pathogen transmission: Prevention and control.* Science of The Total Environment, 2020: p. 142090.

[27] Sadrizadeh, S., et al., *Influence of staff number and internal constellation on surgical site infection in an operating room.* Particuology, 2014. 13: p. 42-51.

[28] Wang, C., S. Holmberg, and S. Sadrizadeh, *Numerical study of temperature-controlled airflow in comparison with turbulent mixing and laminar airflow for operating room ventilation.* Building and Environment, 2018. 144: p. 45-56.

[29] Shih, T.-H., et al., *A new k-ϵ eddy viscosity model for high reynolds number turbulent flows.* Computers & fluids, 1995. 24(3): p. 227-238.

[30] Srebric, J., et al., *CFD boundary conditions for contaminant dispersion, heat transfer and airflow simulations around human occupants in indoor environments.* Building and Environment, 2008. 43(3): p. 294-303.

[31] Chen, Q., *Comparison of different k-ε models for indoor air flow computations.* Numerical Heat Transfer, Part B Fundamentals, 1995. 28(3): p. 353-369.

[32] Zhai, Z.J., et al., *Evaluation of various turbulence models in predicting airflow and turbulence in enclosed environments by CFD: Part 1—Summary of prevalent turbulence models.* Hvac&R Research, 2007. 13(6): p. 853-870.

[33] Van Maele, K. and B. Merci, *Application of two buoyancy-modified k–ε turbulence models to different types of buoyant plumes.* Fire Safety Journal, 2006. 41(2): p. 122-138.

[34] Kuznik, F., G. Rusaouën, and J. Brau, *Experimental and numerical study of a full scale ventilated enclosure: Comparison of four two equations closure turbulence models.* Building and Environment, 2007. 42(3): p. 1043-1053.

[35] Al Assaad, D., et al., *Effectiveness of intermittent personalized ventilation in protecting occupant from indoor particles.* Building and Environment, 2018. 128: p. 22-32.

[36] Zheng, C., et al., *Comparison of air-conditioning systems with bottom-supply and side-supply modes in a typical office room.* Applied Energy, 2018. 227: p. 304-311.

[37] Liu, C., G. Zhou, and H. Li, *Analysis of thermal environment in a hospital operating room.* Procedia Engineering, 2015. 121: p. 735-742.

[38] Oh, W. and S. Kato, *The effect of airspeed and wind direction on human's thermal conditions and air distribution around the body.* Building and Environment, 2018. 141: p. 103-116.

[39] Ning, M., et al., *Computational fluid dynamics (CFD) modelling of air flow field, mean age of air and CO2 distributions inside a bedroom with different heights of conditioned air supply outlet.* Applied energy, 2016. 164: p. 906-915.

[40] Dehghan, M.H. and M. Abdolzadeh, *Comparison study on air flow and particle dispersion in a typical room with floor, skirt boarding, and radiator heating systems.* Building and Environment, 2018. 133: p. 161-177.

[41] Abou Hweij, W., et al., *Optimized performance of displacement ventilation aided with chair fans for comfort and indoor air quality.* Energy and Buildings, 2016. 127: p. 907-919.

[42] Cao, S.-J., et al., *Study on the impacts of human walking on indoor particles dispersion using momentum theory method.* Building and Environment, 2017. 126: p. 195-206.

[43] Ganesh, G.A., S.L. Sinha, and T.N. Verma, *Numerical simulation for optimization of the indoor environment of an occupied office building using double-panel and ventilation radiator.* Journal of Building Engineering, 2020. 29: p. 101139.

[44] Zhang, W., et al., *Numerical study on the gas leakage and dispersion at the street intersection of a building group.* Computer Modeling in Engineering & Sciences, 2020. 123(3): p. 1247-1266.

[45] Rahimi, A., T. Tavakoli, and S. Zahiri, *Computational fluid dynamics (CFD) modeling of gaseous pollutants dispersion in low wind speed condition: Isfahan refinery, a case study.* Petroleum science and technology, 2014. 32(11): p. 1318-1326.

[46] *ASHRAE, ANSI Standard 170-2008 Ventilation of Health Care Facilities*. (2008), American Society of Heating, Refrigerating and Air-Conditioning Engineers, Inc, Atlanta.

[47] *ASHRAE, ANSI Standard 170–2013 Ventilation of Health Care Facilities.* American Society of Heating, Refrigerating and Air-Conditioning Engineers, Inc, Atlanta, 2013.

[48] Uğursal, A. and C.H. Culp, *The effect of temperature, metabolic rate and dynamic localized airflow on thermal comfort.* Applied energy, 2013. 111: p. 64-73.

[49] *ASHRAE, ASHRAE Standard 55-2017. Thermal environmental conditions for human occupancy. ASHRAE. Atlanta; (2017).*

[50] Fanger, P.O., *Thermal comfort. Analysis and applications in environmental engineering.* Thermal comfort. Analysis and applications in environmental engineering., 1970.

[51] Yao, Y., et al., *Experimental study on skin temperature and thermal comfort of the human body in a recumbent posture under uniform thermal environments.* Indoor and Built Environment, 2007. 16(6): p. 505-518.

[52] *ISO 7730, Ergonomics of the thermal environment-Analytical determination and interpretation of thermal comfort using calculation of the PMV and PPD indices and local thermal comfort criteria*. (2005).

[53] Liu, W., Z. Lian, and Y. Yao, *Optimization on indoor air diffusion of floor-standing type room air-conditioners.* Energy and buildings, 2008. 40(2): p. 59-70.